RSC Advances

PAPER

View Article Online
View Journal | View Issue

Cite this: *RSC Adv.*, 2024, **14**, 7459

Effect of destability time on microstructure and properties of hypoeutectic high chromium cast iron

Lingyun Xiong,[ac] Yaru Liu,*[ab] Qing Zeng,[d] JianPing Lai[e] and Xiang Qiao[f]

Received 18th February 2024
Accepted 26th February 2024

DOI: 10.1039/d4ra01247j

rsc.li/rsc-advances

The present work investigated the effect of destabilization time on the mechanical properties and microstructure evolution of high chromium cast iron, and scanning electron microscopy and electron probe microanalysis techniques were employed. The results show that the hardness of hypoeutectic high chromium cast iron is related to the size and volume fraction of secondary carbides precipitated from the matrix. The hardness of the alloy continues to rise due to the continuous increase of the volume fraction of the secondary carbide at the initial stage of destabilization. The alloy reaches its peak hardness value at 950 °C and 1000 °C for 1 hour holding time. The solid solubility of carbon and alloying elements in the matrix increases as the holding time extends, resulting in a large number of carbides redissolved into the matrix, making the hardness of the alloy decrease; the hardness of the alloy at 14 h is less than that at 10 min. Under 1050 °C, the size and density of the secondary carbide increase significantly; extending the holding time will lead to the continuous reduction of the carbide rod that provides strength, thus, the hardness curve shows a downward trend.

1 Introduction

Due to its excellent wear resistance, high chromium cast iron is widely used in various wear-resistant fields, such as the power industry, metallurgy, building materials and agricultural fields, and has obtained good economic benefits. With its exceptional wear resistance, high chromium cast iron is widely applied in various wear-resistant sectors, encompassing industries like power, mining, metallurgy, building materials, and agriculture.[1–3] Currently, the properties, morphology, and distribution of carbides in the structure, as well as the matrix structure of high chromium cast iron, are enhanced through various techniques such as alloying, metamorphic treatment, and optimized heat treatment. These approaches are utilized to enhance the material's performance, resulting in improved properties and a more refined microstructure.[4]

Most high chromium cast iron is used in the heat treatment state, which is an important means to maximize the wear resistance of high chromium cast iron. The purpose of heat treatment is to enhance the structural arrangement within the material, thus enabling it to achieve an optimal balance of strength, toughness, and wear resistance. Additionally, heat treatment can also be applied to soften the material and enhance the cutting performance of the alloy.[5] The as-cast matrix of high chromium cast iron typically consists of a significant proportion of residual austenite and a minor amount of sheet martensite.[6–8] The reason for the formation of residual austenite is due to the fast cooling rate of the casting, the element is not enough to diffuse, resulting in a large amount of carbon and alloying elements in the matrix, which makes the material hardenability increase at the same time, but also makes the martensitic phase transition temperature (M_s) drop below room temperature, and the austenitic structure is retained to room temperature.[9] The residual austenite in the as-cast state has a high concentration of carbon and chromium, the distribution of elements inside the grain is uneven and in a susaturated state, also the stability is poor. Once the thermodynamic conditions are mature, it will be transformed to a stable state, so high chromium cast iron needs to be heat treated to meet the requirements of use. By heat treatment process, these alloying elements are precipitated from susaturated matrix in the form of secondary carbide so that the matrix reaches a stable state. The distribution of secondary carbides (volume fraction, density and size) has an important effect on the wear resistance of high chromium cast iron.[10–13]

At present, the annealing process of high chromium cast iron is the most widely used process. Destabilization refers to the process where carbon and alloying elements in the matrix

[a]*National Key Laboratory of Green and Long-Life Road Engineering in Extreme Environment (Changsha), Changsha University of Science & Technology, Changsha, 410114, Hunan, China*

[b]*School of Traffic & Transportation Engineering, Changsha University of Science and Technology, Changsha 410114, China*

[c]*Chengnan College, Changsha University of Science and Technology, Changsha 410114, China*

[d]*School of Physics & Electronic Science, Changsha University of Science and Technology, Changsha 410114, China*

[e]*Key Laboratory of Testing Technology for Manufacturing Process in Ministry of Education, State Key Laboratory of Environment-friendly Energy Materials, Southwest University of Science and Technology, Mianyang, 621010, China*

[f]*Markets Supervision Administration of Changsha County, Changsha 410100, China*

precipitate as secondary carbides due to the unstable supersaturated residual austenite, under the influence of temperature. This results in the transformation of the matrix to achieve a stable microstructure.[14–16] High chromium cast iron usually contains a large number of residual austenite structure, which contains a large number of carbon and alloying elements and will lead to the component segregation. If not eliminated or improved in time, the metastable structure will transformation into martensite, accompanied by a large phase change stress, leading to workpiece cracking or falling. The optimization of the heat treatment process primarily involves controlling the composition of the matrix phase and the characteristics of secondary carbides, such as their size, volume fraction, and density.[17,18] This is achieved by carefully adjusting the temperature and duration of the treatment in order to effectively control the strength, toughness, and wear resistance of high chromium cast iron. With prolonging of destabilization time, the precipitation rate of secondary carbides enhanced, the content of secondary carbides in the matrix continues to increase, as well as the hardness and wear resistance of the material.[19] However, if the temperature is too high or the holding time is too long, the solid solubility of carbon and alloying elements will heighten, leading to the dissolution of the secondary carbides, resulting in a large number of carbon and alloying elements. As the content of residual austenite increases, the hardness of the matrix decreases. Therefore, it is very important to explore a balanced destabilization system to regulate the precipitation of secondary carbides and the phase ratio of the matrix in the destabilization heat treatment.[20–23]

Traditionally, X-ray diffraction (XRD) and other single-phase analysis methods are commonly employed to investigate the impact of second-phase particles on the microstructure and properties of hypoeutectic high-chromium cast iron. The precipitation of secondary carbides in the heat preservation can be divided into nucleation stage and coarsening and growing stage.[24] The length of nucleation stage depends on the level of the destabilization temperature. Enhancing the destabilization temperature will lead to the increase of the atomic diffusion rate as well as the nucleation and precipitation rate of the secondary carbides.[25] If the destabilization temperature is the temperature range dominated by the precipitation of secondary carbides, the extension of holding time is conducive to the thorough precipitation of secondary carbides, and the content of carbon and alloying elements in austenite is close to the solubility under equilibrium conditions. Similarly, if the destabilization temperature is the temperature range dominated by the precipitation and dissolution of secondary carbides, with the extension of time, the dissolution of secondary carbides will be more complete and thorough, and the content of residual austenite will increase.[26,27] However, these methods do not provide insights into the mechanisms underlying the influence of destabilization treatment on the secondary carbides within the matrix, as well as the regulatory patterns of the precipitated phase components within the matrix.

In this paper, Electron Probe Micro-Analyzer (EPMA), Scanning Electron Microscope (SEM) and other detection techniques were employed to examine how the destabilization temperature and time affect the precipitation characteristics (size, morphology, and volume fraction) of secondary carbides within the matrix during destabilizing heat treatment. By employing nucleation theory and observing the morphology and quantity of matrix precipitates at different times, the influence of extending holding time on the size and quantity of secondary carbides at three temperatures was discussed. Results confirms that controlling the destabilization conditions is a crucial factor in achieving the desired morphology and performance of the precipitates. The continuous extension of holding time reduce the integral number of secondary carbides, increase the residual austenite, and finally make the alloy hardness increase first and then decrease.

2 Materials and methods

Tests were performed with high carbon steel specimens with the following composition (wt%): 2.8% C, 0.28% Si, 0.61% Mn, 18.2% Cr and balance Fe. After deoxidation, the high carbon steel was melted using medium-frequency induction in a furnace and then cast into ingots. Based on the results of the spectral composition test, the composition of the high carbon steel is adjusted before it is placed in the furnace. The temperature is carefully controlled within the range of 1500 to 1540 °C, and the pouring temperature is controlled within the range of 1380 to 1400 °C. For casting, a $\Phi 200 \times 300$ mm metal mold is used with a mold thickness of 20 mm. The material used for the mold is Q235 steel.

In this paper, Rockwell hardness (HRC) is tested by using diamond indenter on HBRVU-187.5 Brovier optical hardness tester, and the load is 1471 N. The matrix hardness was characterized by Vickers hardness (HV), and the hardness was tested by microindentation hardness tester (BUEHLER5104). The Sirion 200 field emission SEM equipment produced by FEI Company was used to observe the high-power microstructure of high-chromium cast iron in the as-cast and heat-treated states, and the micro-region composition analysis was carried out with the supporting EDAX energy spectrum analyzer, the accelerated voltage was 20 kV. The electron probe can quantitatively analyze the chemical composition of the small region (micron level) in the sample, especially for the analysis of light elements (C, N,

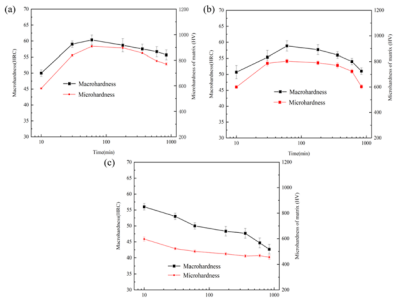

Fig. 1 The curves of hardness with soaking time at different destabilization temperatures (a) 950 °C; (b) 1000 °C; (c) 1050 °C.

etc.), which has a higher accuracy than EDS spectrum. Therefore, the electron probe analyzer in this paper adopts JMA-8230 of Nippon Electronics, the acceleration voltage is 30 kV, and the luminous filament is lanthanum hexaboride.

3 Results

3.1 Mechanical property

Fig. 1 shows the hardness change curve of the alloy held at 950–1050 °C for different times (10 min, 30 min, 1 h, 3 h, 6 h, 10 h, 14 h). In order to reveal the contribution weight of matrix hardness

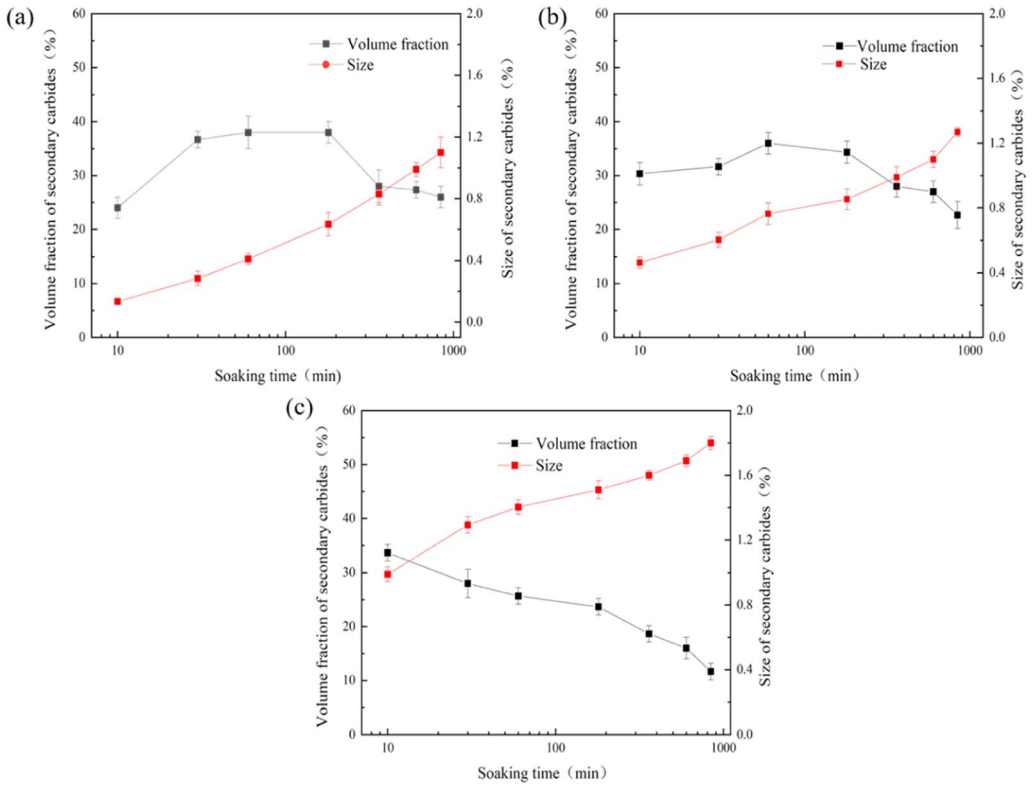

Fig. 2 The curves of size and volume fraction of secondary carbides with soaking time (a) 950 °C; (b) 1000 °C; (c) 1050 °C.

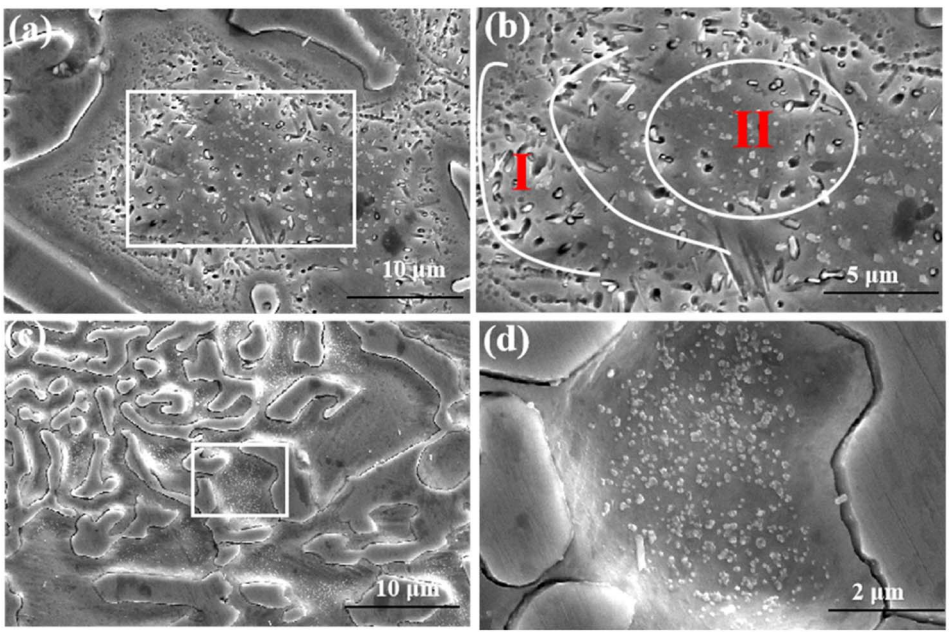

Fig. 3 The matrix and eutectic microstructure of the alloy treated at 950 °C for 20 min (a and b) matrix microstructure; (c and d) eutectic microstructure.

to macroscopic hardness, the micromechanical properties of particles are also investigated. As can be seen from the figure, the curve changes at 950 °C and 1000 °C are similar. During the incubation period of 10 min to 1 h, the hardness rises rapidly, and the hardness reaches the peak value when the incubation period is 1 h. The peak hardness at 950 °C (62HRC) is higher than that at 1000 °C (59.5HRC). With the extension of holding time (1–14 h), the hardness showed a slow decline trend, and the hardness decline of 1000 °C was greater than that of 950 °C. At 1000 °C, the hardness of the alloy decreases from 59.5HRC at 1 h to 52HRC at 14 h, while when the temperature kept at 950 °C, the hardness of the alloy decreases from 62HRC at 1 h to 57HRC at 14 h. Different from the curve changes at 950 °C and 1000 °C, the hardness curve at 1050 °C shows a decreasing trend, and the hardness of the alloy decreases from 55HRC at the initial stage of insulation (10 min) to 43HRC at 14 h.

3.2 Microstructure evolution

Fig. 2 shows the change curves of the size and volume fraction of secondary carbides precipitated from the matrix at 950–1050 °C for different time (10 min, 30 min, 1 h, 3 h, 6 h, 10 h, 14 h). It can be seen from the figure that the variation curve of the volume fraction of secondary carbide and the hardness curve are the same. The volume fraction of secondary carbides at 950 °C and 1000 °C increased continuously from 10 min to 1 h, and reached a peak value at 1 h. The peak volume fraction at 950 °C (41%) was greater than that at 1000 °C (36%). However, in the initial stage of insulation (10 min), the volume fraction of secondary carbide at 1000 °C (31%) is greater than that at 950 °C (26%). Increasing the insulation time from 1 hour to 14 hours results in a gradual decrease in the volume fraction of secondary carbides. At 950 °C, the volume fraction decreases from 41% after 1 hour of insulation to 28% after 14 hours. Similarly, at 1000 °C, the volume fraction decreases from 36%

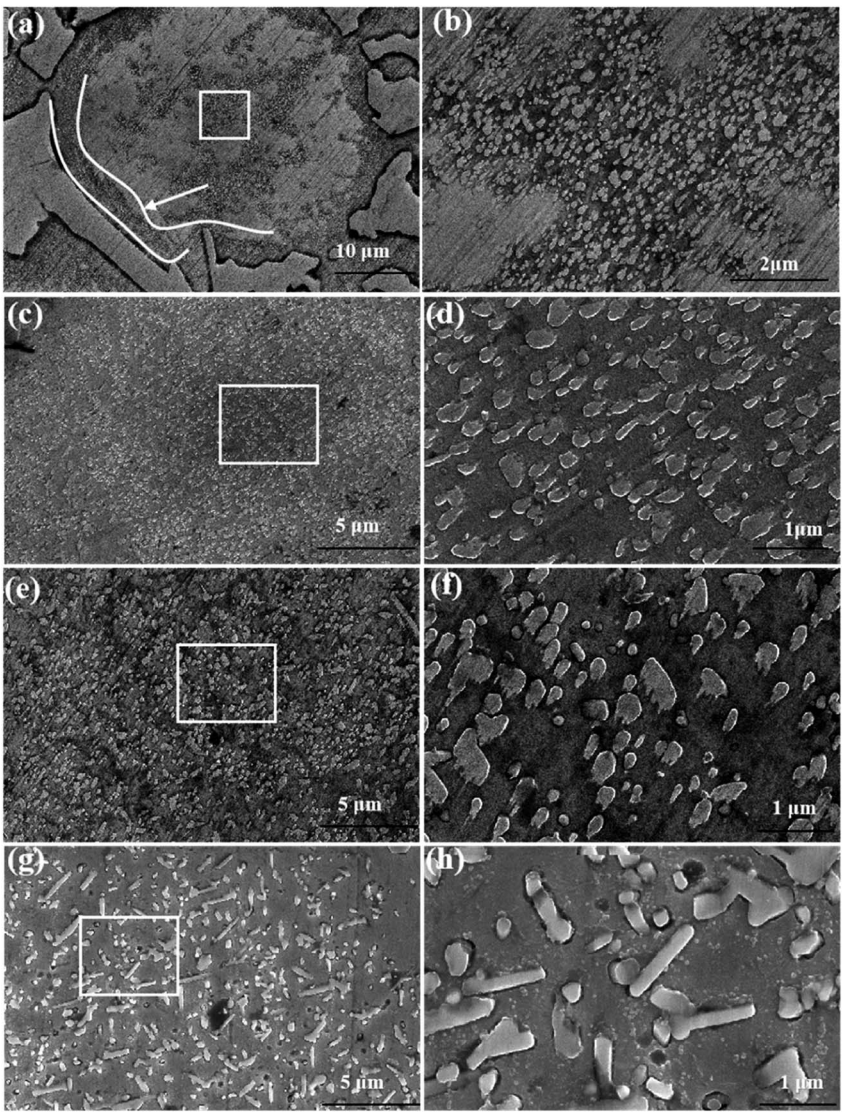

Fig. 4 SEM images of secondary carbides treated at 950 °C for different time (a and b) 10 min; (c and d) 1 h; (e and f) 3 h; (g and h) 14 h.

after 1 hour of insulation to 23% after 14 hours. These results indicate that with prolonged insulation time, the formation of secondary carbides gradually decreases. The volume fraction of secondary carbide at 1050 °C is also the same as the hardness curve, which decreases from 35% for 10 min to 13% for 14 h. At all three temperatures, the size of the secondary carbides shows an increasing trend. When the insulation time is increased from 10 minutes at 950 °C to 14 hours, the size of the secondary carbides increases from an initial value of 0.15 μm to 1.1 μm. Similarly, at the same insulation duration, at 1000 °C, the size of the secondary carbides increases from 0.5 μm to 1.3 μm, resulting in a 260% increase. However, at 1050 °C, when the insulation time is extended to 14 hours, the size only increases by 1 μm compared to 10 minutes.

3.2.1 Microstructure evolution of tested alloy at 950 °C. Fig. 3 shows the precipitated morphology of the matrix and eutectic structure at 950 °C for 20 min. It can be seen from the figure that a large number of nanoscale secondary carbides are precipitated in both the matrix and the eutectic structure, but the morphologies of secondary carbides precipitated in the matrix in different regions are different. The interface region between matrix and eutectic carbide (I region) and the middle region of matrix (II region) are taken as examples, as shown in Fig. 3(b), the density of precipitated phase in region I is much higher than that in region II, meanwhile, the color contrast of secondary carbides in region I is whiter than that in region II. However, for region II, the precipitated phase has a small density, granular and square morphology with dark contrast, and the austenite has not been completely decomposed. As can be seen from Fig. 3(d), a large number of granular secondary carbides of nanometer size are also precipitated in the matrix region between the eutectic carbides.

Fig. 4 shows the precipitated morphology of the matrix at 950 °C for holding time. As shown in Fig. 4(a) and (b), when the insulation time is 10 minutes, secondary carbides continuously precipitate from the substrate, accompanied by the decomposition of some remaining austenite. The precipitation of secondary carbides starts from the edges of the matrix (as indicated by the arrows) and progresses along the center of the matrix. As time progresses, the quantity of precipitated secondary carbides continuously increases, and their volume fraction reaches a maximum after 1 hour of insulation. When the insulation time is increased from 1 hour to 3 hours, the secondary carbides begin to coarsen, and their density and volume fraction slightly decrease. Additionally, a small amount of rod-like secondary carbides with an aspect ratio of around 2–3 and a length of 0.7–0.9 μm is observed by Image J software. When the insulation time reaches 14 hours, the secondary carbides continue to coarsen, and the content of rod-like secondary carbides increases. The length of the rod-like secondary carbides also increases to the range of 1.3–1.8 μm.

3.2.2 Microstructure evolution of tested alloy at 1000 °C. Fig. 5 exhibited the morphology of the base structure after different insulation time at 1000 °C. As shown in the figure, the amount and size of secondary carbides precipitated from the matrix are larger than those at 950 °C in the same period when the heat is held for 10 min, the residual austenite in the as-cast state has basically decomposed completely. Different from 950 °C, the secondary carbide held at 1000 °C for 10 min contains rod and granular morphologies. When the holding time reached to 1 h, the size and volume fraction of the secondary carbide increase synchronously, and the volume fraction get to a peak value. With an extended insulation time of 10 hours, the coarsening of the secondary carbides in the matrix becomes more pronounced, with a noticeable decrease in both

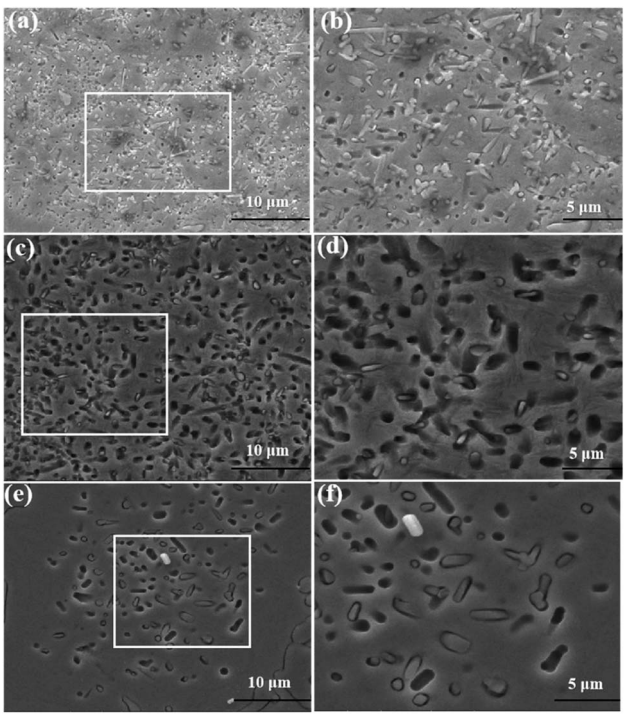

Fig. 5 SEM images of secondary carbides treated at 1000 °C for different time (a and b) 10 min; (c and d) 1 h; (e and f) 10 h.

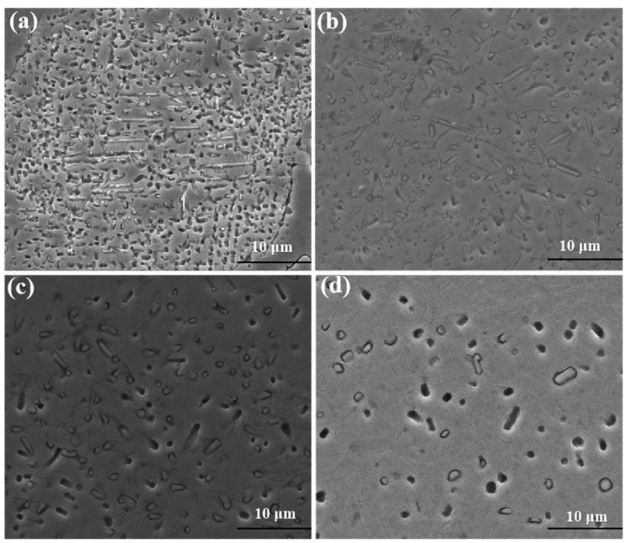

Fig. 6 SEM images of secondary carbides treated at 1050 °C for different time (a) 10 min; (b) 1 h; (c) 6 h; (d) 10 h.

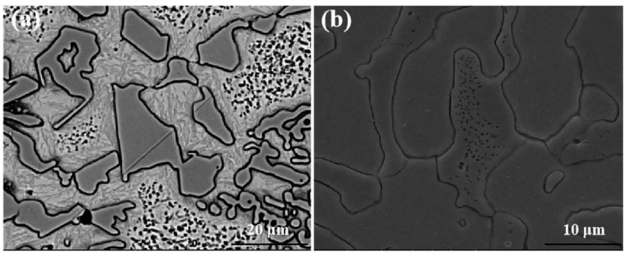

Fig. 7 Microstructure of eutectic carbides treated at 1050 °C for 1 h and 14 h (a) 1050 °C for 1 h; (b) 1050 °C for 10 h.

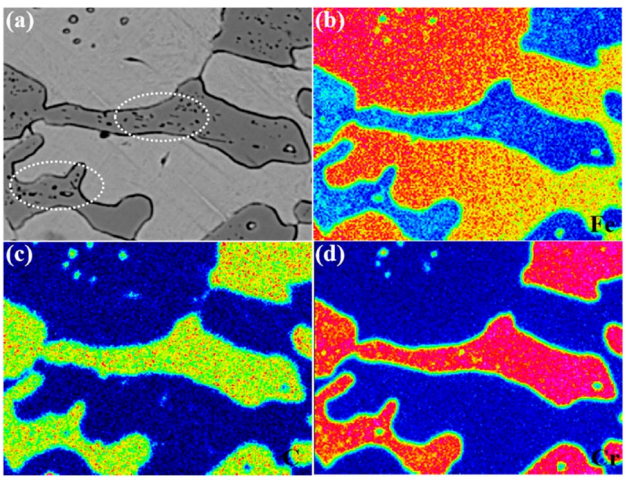

Fig. 8 EPMA mapping microstructure of eutectic carbides treated at 1050 °C for 10 h (a) microstructure; (b) mapping of Fe; (c) mapping of C; (d) mapping of Cr.

the distribution density and volume fraction. The length of the rod-like carbides measures between 1.6 and 2.0 μm.

3.2.3 Microstructure evolution of tested alloy at 1050 °C. Fig. 6 displays the microstructure of the matrix of the alloy after insulation at 1050 °C for varying amounts of time. As illustrated in the figure, after 10 minutes of insulation, the density of the secondary carbides precipitated in the matrix is at its highest, surpassing those formed at 950 °C and 1000 °C in terms of size and density. The morphology of the carbides precipitated in the center of the matrix is primarily rod-shaped, with a length ranging from 2.5 to 3.0 μm. With increase the insulation time, the length of the rod-like carbides decreases continuously, while the width increases. Both the density and volume fraction of the secondary carbides show a significant decrease. Additionally, the corrosion resistance of the sample enhanced, and the time for the sample color to turn gray during corrosion process is obviously longer.

According to the current literature reports,[26] M_7C_3 eutectic carbides do not change during the destabilization heat treatment process. Fig. 7 shows the morphologies of eutectic carbides held at 1050 °C for 1 h and 10 h. As shown in the figure, the eutectic carbide did not change at 1050 °C for 1 h, and the surface of the carbide was smooth with sharp and clear edges. When the holding time reached 10 h, the edges and corners of the eutectic carbide appeared inactive. Compared with the morphology of the eutectic carbide held for 1 h, the sharp edges and corners became smooth, and some of the eutectic carbides showed micropore morphology inside.

Fig. 8 shows EPMA plane analysis of eutectic carbides held at 1050 °C for 10 h. As shown in the figure, the second phase particles are precipitated inside the eutectic carbide, the size of that is nanometer, and its components are mainly carbon, chromium and iron, possibly M_3C, M_7C_3 or $M_{23}C_6$. Due to the size of the eutectic carbide, the probe cannot quantitatively analyze its composition, and the kinetics and types of its precipitation need to be further studied.

4 Discussion

According to the research results of Efremenko[28] on the precipitation behavior of secondary carbides in high chromium cast iron, the precipitation of secondary carbides in the process of destabilization heat treatment can be divided into nucleation stage and coarsening growth stage, and the coarsening growth stage is the Ostwald ripening process. When the size and volume fraction of secondary carbides precipitated from the matrix increase synchronously, it indicates that the nucleation stage begins at this time. While if the size of the secondary carbide increases, but the total volume fraction decreases, the grain begins to enter the coarsening and growing stage. It can be seen from Fig. 1 that at 950 °C and 1000 °C, the nucleation stage of crystal nucleus is 0-1 h, and the crystal nucleus continues to coarsen and grow in the following 13 hours. In contrast, at 1050 °C, the crystal nucleus mainly forms in the first 10 minutes and grows in the following holding time.

Fig. 9 shows the influence of destability time and temperature on the precipitated phase of the matrix. As shown in the figure, in the first ten minutes of heat preservation, the size and content of secondary carbides precipitated from the matrix at

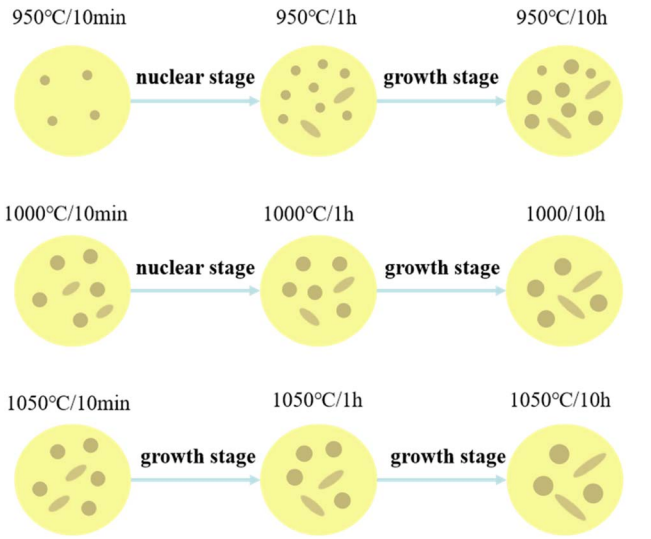

Fig. 9 Effection of destabilization conditions on the secondary carbides precipitated.

different temperatures are different, and the rule is 1050 °C > 1000 °C > 950 °C. From the nucleation theory it can be observed that, the higher the temperature, the faster the diffusion rate, the faster the nucleation rate, the larger the critical nucleation size and the larger the volume fraction.[29] For 950 °C, 1000 °C and 1050 °C, all belong to the nucleation stage, the size and volume fraction of secondary carbides increase synchronically. With the increase of temperature, the higher the nucleation rate, the larger the critical nucleation size, as a result, the size and volume fraction of secondary carbides at 1050 °C are the largest. At the same time, it can be observed from Fig. 3 that the size and density of secondary carbides in the nucleation stage in the surrounding region of the matrix are larger than that in the middle region of the matrix. This is because the thermal expansion coefficients of the matrix and eutectic carbides are different. In the process of temperature change, a large number of crystal defects such as lattice vacancies, dislocations and slip bands appear. These crystal defects reduce the nucleation work of secondary carbides, greatly increase the diffusion rate of atoms, and longer destabilization times result in an increase in the chromium-to-carbon ratio of secondary carbides, longer lengths of rod-like secondary carbides, and a higher overall content of these secondary carbides.

At the same time, it can be observed from Fig. 3 that the size and density of secondary carbides in the nucleation stage in the surrounding region of the matrix are larger than that in the middle region of the matrix. This is because the thermal expansion coefficients of the matrix and eutectic carbides are different. In the process of temperature change, a large number of crystal defects such as lattice vacancies, dislocations and slip bands appear. These crystal defects reduce the nucleation work of secondary carbides, greatly increase the diffusion rate of atoms, and lead to larger critical nucleation size and faster nucleation rate of secondary carbides in the region around the matrix.

With the extension of holding time to 1 h, the volume fraction of secondary carbides precipitated from the matrix at 950 °C and 1000 °C reaches the peak value, and the volume fraction of secondary carbides precipitated from the matrix at 950 °C is greater than 1000 °C, which is because the solid solubility of carbon and alloy elements in the matrix at 1000 °C is greater than 950 °C. When the holding time increases from 10 min to 1 h, the secondary carbides enter the coarsening and growing stage at 1050 °C, and the secondary carbides are further coarsened and the volume fraction is further reduced. When the holding time increases from 1 h to 10 h, the secondary carbides in the matrix enter the coarsening and growing stage under all temperature conditions. The higher the temperature, the faster the coarsening rate and the lower the volume fraction in the matrix. Owing to the higher the temperature, the greater the solid solubility of carbon and alloying elements in the matrix.

The secondary carbides precipitated from the matrix in the process of destabilizing heat treatment can be divided into rod shape and granular shape. According to the previous research results, the chrome-carbon ratio of secondary carbides is the key factor affecting the morphology of secondary carbides, and the higher the chrome-carbon ratio, the more rod-shaped the morphology. Powell[30] believe that the granular secondary carbide precipitated at the initial stage of destabilization is $M_{23}C_6$, and the rod-shaped secondary carbide is M_7C_3. With the extension of time, the granular $M_{23}C_6$ carbide is transformed into rod-shaped M_7C_3 carbide *in situ*, and the orientation relationship is $[100]M_{23}C_6//[100]M_7C_3$. The crystal face relation is $(015)M_{23}C_6//(010)M_7C_3$. The influence of destability temperature and time on the precipitated phase of the matrix is confirmed from the chemical point of view, according to the equilibrium phase diagram calculated by Mohsen Mohammadi Zahrani and Guangxin Wu,[31,32] in the composition of hypo-eutectic high-chromium cast iron with a chromium content of 15–20 wt%, the stable phase of the secondary carbides precipitated from the matrix is M_7C_3 carbides, while $M_{23}C_6$ carbides or M_3C carbides are an unstable transition carbides. The granular secondary carbides may be $M_{23}C_6$ carbides or M_3C carbides in the initial stage of instability, and extending the holding time will make the metastable $M_{23}C_6$ carbides or M_3C carbides transform into stable rod-shaped M_7C_3 carbides. When the holding time is less than 1 hour, the initial metastable $M_{23}C_6$ carbides or M_3C carbides continue to transform into stable M_7C_3 carbides, and the rod-shaped secondary carbides continue to increase. When the holding time is increased to 10 h, the Cr/C ratio of rod-shaped M_7C_3 carbides continues to increase, and the length of carbides also continues to increase. It can be seen that extending the holding time or increasing the holding temperature will accelerate the atomic diffusion rate, and the proportion of stable rod-shaped M_7C_3 carbide will increase, resulting in a decrease in matrix hardness. This conclusion confirms that controlling the destabilization conditions is a crucial factor in achieving the desired morphology and performance of the precipitates.

5 Conclusion

(1) At temperatures of 950 °C and 1000 °C, the hardness curve of the alloy shows an initially increasing and then decreasing trend. The peak hardness is reached after a 1 h holding time. Prolonging the holding time results in a decrease in alloy hardness. After 14 hours, the alloy's hardness at 950 °C decreases less than at 1000 °C.

(2) Under different tempering conditions, the content and size of secondary carbides precipitated in the matrix differ, and follow a pattern of 1050 °C > 1000 °C > 950 °C.

(3) The hardness of the matrix primarily depends on the content and distribution of martensite, as well as the volume fraction and size of secondary carbides precipitated on the martensite. When the volume fraction of secondary carbides is at its maximum and the size is the smallest, the matrix achieves its highest hardness.

Author contributions

Lingyun Xiong: investigation, experiment; Yaru Liu: data analysis, writing; Qing Zeng: supervision, review; JianPing Lai: discussion, supervision, consulting, proposal; Xiang Qiao: supervision, review.

Conflicts of interest

The authors declare no known competing financial interests or personal relationships that could have appeared to influence the work reported in this paper.

Acknowledgements

This work was supported by National Natural Science Foundation of China (No. 52208422), Open Fund of National Key Laboratory of Green and Long-Life Road Engineering in Extreme Environment (Changsha University of Science & Technology) (No. kfj230113), the Scientific Research Project of Hunan Education Department (No. 21B0311) and National College Student Innovation Training Program Project (No. S202313635002).

References

1 X. Cheng, D. Zhang and X. Wu, Effect of quenching holding time on the microstructure and properties of high silicon hypereutectic high chromium cast iron, *Surf. Rev. Lett.*, 2023, (9), 30.
2 P. A. Santhosh and P. T. Parameshwaran, Influence of hybrid nanoparticles on the wear behavior of aluminum alloy composites for aerospace applications, *Ind. Lubr. Tribol.*, 2023, **75**(2), 204–210.
3 V. B. Rucker, G. D. S. Balbinot, F. M. Collares, *et al.*, Synthesis of silver core-shell nanoparticles and their influence on an experimental resin endodontic sealer: an in vitro analysis, *Int. Endod. J.*, 2023, **56**(2), 289–303.
4 M. S. Raksha, B. Adaveesh, M. Nagaral, *et al.*, Impact of Boron Carbide Particles and Weight Percentage on the Mechanical and Wear Characterization of Al2011 Alloy Metal Composites, *ACS Omega*, 2023, **8**(26), 23763–23771.
5 K. H. Zeytin, H. Yildirim, B. Berme, *et al.*, Effect of boron and heat treatment on mechanical properties of white cast iron for mining application, *ISIJ Int.*, 2011, **18**, 31–39.
6 A. N. Sudhakar, R. Markandeya and B. Srinivasa Rao, Effect of alloying elements on the microstructure and mechanical properties of high chromium white cast iron and Ni-Hard iron, *Mater. Today: Proc.*, 2022, **3**(61), 1006–1014.
7 K. Chen, J. Zhang and X. Chen, The effect of iron on the microstructure and mechanical properties of a cast Cu-12Sn-1.5Ni(wt.%) alloy, *Mater. Sci. Eng., A*, 2020, **21**(758), 139330.
8 Y. Z. Lv, Y. F. Sun, J. Y. Zhao, *et al.*, Effect of tungsten on microstructure and properties of high chromium cast iron, *Mater. Des.*, 2012, **39**, 303–308.
9 S. Imurai, C. Thanachayanont, J. T. H. Pearce, *et al.*, Effect of Mo on microstructure of as-cast 28wt.%Cr-2.6wt.%C-(0-10) wt.% Mo irons, *Mater. Charact.*, 2014, **90**, 99–102.
10 H. Jiang, X. Zhang and R. Yang, Microstructure evolution and mechanical behavior of Cu-7Ni-7Al-4Fe-2Mn alloy via a quenching-aging heat treatment, *Mater. Today Commun.*, 2024, **3**(38), 108152.
11 S. Liu, Y. F. Zhou, X. L. Xing, *et al.*, Refining effect of TiC on primary M_7C_3 in hypereutectic Fe-Cr-C harden-surface welding coating: experimental research and first-principles calculation, *J. Alloys Compd.*, 2017, **691**, 239–249.
12 S. Liu, Z. J. Wang, Z. J. Shi, *et al.*, Experiments and calculations on refining mechanism of NbC on primary M_7C_3 carbide in hypereutectic Fe-Cr-C alloy, *J. Alloys Compd.*, 2017, **713**, 108–118.
13 Q. Miao, W. Ding, Y. Gu, *et al.*, Comparative investigation on wear behavior of brown alumina and microcrystalline alumina abrasive wheels during creep feed grinding of different nickel-based superalloys, *Wear*, 2019, **426–427**, 1624–1634.
14 G. Xiao, Y. Zhang and B. Zhu, Wear behavior of alumina abrasive belt and its effect on surface integrity of titanium alloy during conventional and creep-feed grinding, *Wear*, 2023, **2**(15), 514–515.
15 H. Pourasiabi and J. D. Gates, Effects of matrix chromium-to-carbon ratio on high-stress abrasive wear behavior of high chromium white cast irons dual-reinforced by niobium carbides, *Tribol. Int.*, 2022, **167**, 107350.
16 X. Liu, G. Zhou and Y. Y. Shen, Evolution of primary carbides during accelerated solidification process of high-carbon martensitic stainless steels, *J. Mater. Res. Technol.*, 2023, **23**, 5935–5944.
17 O. Haiko, S. Pallaspuro and V. Javaheri, High-stress abrasive wear performance of medium-carbon direct-quenched and partitioned, carbide-free bainitic, and martensitic steels, *Wear*, 2023, **8**(15), 526–527.
18 J. P. Lai, Q. L. Pan, H. J. Peng, *et al.*, Effects of Si on the microstructures and mechanical properties of high-chromium cast iron, *J. Mater. Eng. Perform.*, 2016, **25**, 4617–4623.
19 Z. Wu, K. Ushioda and H. Fujii, Mechanism of suppressing HAZ softening in friction stir welded martensitic steel through hardening phenomenon initiated by adding vanadium, *J. Mater. Res. Technol.*, 2023, **9**(26), 1151–1211.
20 X. S. Jia, Q. G. Hao, X. W. Zuo, *et al.*, High hardness and toughness of white cast iron: The proposal of a novel process, *Mater. Sci. Eng., A*, 2014, **68**, 96–103.
21 L. M. Meng, J. G. Ding and Z. S. Dong, Prediction of roll wear and thermal expansion based on informer network in hot rolling process and application in the control of crown and thickness, *J. Manuf. Process.*, 2023, **10**(6), 248–260.
22 D. Zhang and L. Zhao, Experimental study on heat transfer and flow resistance characteristics of integral rolled spiral finned tube bundles heat exchangers, *Case Stud. Therm. Eng.*, 2023, **52**(9), 103689.
23 C. Wu, L. Zhang and P. Qu, HD-lubricated high-speed small reduction rolling of hard steel strips with elastically deformable work rolls, *Tribol. Int.*, 2022, **165**, 107295.
24 C. Wu, L. Zhang and P. Qu, A numerical strategy for predicting the interface stresses in metal strip rolling with small reduction, *Int. J. Mech. Sci.*, 2023, **240**, 107953.
25 C. Song, J. Cao and J. Xiao, Control strategy of multi-stand work roll bending and shifting on the crown for UVC hot

rolling mill based on MOGPR approach, *J. Manuf. Process.*, 2023, **8**(56), 832–843.
26 M. Andersson, R. Finnstrom and T. Nylen, Introduction of enhanced indefinite chill and high speed rolls in European hot strip mills, *Ironmaking Steelmaking*, 2004, **31**(5), 383–388.
27 R. Nawata, K. Maruta and K. Kojo, Influence of alloying elements on temper softening property of adamite roll, *Trans. Iron Steel Inst. Jpn.*, 1985, **25B**(11), 319–322.
28 V. G. Efremenko, Y. G. Chabak and M. NBrykov, Kinetic parameters of secondary carbide precipitation in high-Cr white iron alloyed by Mn-Ni-Mo-V complex, *J. Mater. Eng. Perform.*, 2013, **22**, 1378–1385.
29 A. Bedolla-Jacuinde, L. Arias and B. Hernandez, Kinetics of secondary carbides precipitation in a high-chromium white iron, *J. Mater. Eng. Perform.*, 2003, **12**, 371–382.
30 G. L. F. Powell and G. Laird, Structure, nucleation, growth and morphology of secondary carbides in high-chromium and Cr-Ni white irons, *J. Mater. Sci.*, 1992, **27**, 29–35.
31 M. M. Zahrani, M. Ketabchi and E. Ranjbarnodeh, Microstructure development and mechanical properties of a C-Mn-Si-Al-Cr cold rolled steel subjected to quenching and partitioning treatment, *J. Mater. Res. Technol.*, 2023, **22**, 2806–2818.
32 G. Wu, Y. Liu and X. Jin, Insight into internal oxidation mechanism of hot rolled Si–Mn added high strength steel: pure iron layer formation, *Vacuum*, 2023, **210**, 111828.